PCCP

PAPER

View Article Online
View Journal | View Issue

Cite this: *Phys. Chem. Chem. Phys.*, 2026, **28**, 7384

Rotational excitation of molecules in the regime of strong ro-vibrational coupling: a comparison between an optical centrifuge and a transform-limited pulse

J. M. García-Garrido,[a] V. Milner,[b] C. P. Koch [c] and R. González-Férez *[ad]

Received 31st July 2025,
Accepted 11th December 2025

DOI: 10.1039/d5cp02931g

rsc.li/pccp

We investigate theoretically the ability of an optical centrifuge, a laser pulse whose linear polarization is rotating at an accelerated rate, to control molecular rotation in the regime when the rigid-rotor approximation breaks down due to coupling between the vibrational and rotational degrees of freedom. Our analysis demonstrates that the centrifuge field enables controlled excitation of high rotational states while maintaining relatively low spread along the vibrational coordinate. We contrast this to the rotational excitation by a linearly polarized Gaussian pulse of equal spectral width and pulse energy, which, although comparable to the centrifuge-induced rotation, is unavoidably accompanied by a substantial broadening of the vibrational wavepacket.

1 Introduction

Laser pulses have long been used for controlling the rotation of molecules.[1–4] Among multiple approaches to rotational control, the method of an optical centrifuge proved to be the most successful in spinning molecules to extremely high rotational states, known as molecular super-rotors.[5,6] The centrifuge is a linearly polarized laser pulse, whose polarization vector rotates with constant angular acceleration. An interaction of the laser-induced dipole moment with the applied laser field results in a torque, which forces the molecule to follow the accelerated rotation of the field polarization.

On the experimental side, optical centrifuges have been used in numerous studies of molecular structure and molecular dynamics (for recent reviews, see ref. 7 and 8). In these investigations, it has been assumed that the centrifuge drives the molecule up the rotational ladder of states, without explicitly driving Raman transitions up the vibrational manifold. This approximation is well justified in the case of relatively light molecular species with strong molecular bonds and correspondingly high energies of Raman-active vibrational modes (*i.e.* >1000 cm^{-1}), which fall outside the available energy bandwidth of amplified femtosecond laser pulses (~ 500 cm^{-1}).

In the case of heavier molecules, or those with softer molecular bonds, ro-vibrational coupling may significantly change the dynamics of a super-rotor. Previous theoretical studies have explored this scenario in the context of the centrifuge-induced dissociation,[9–11] as well as the dissociation induced by a short laser pulse.[12] Interestingly, the reverse process of creating a molecular bond can also be facilitated by the ro-vibrational coupling.[13] On the experimental side, evidence of the ro-vibrational energy exchange in the field-free dynamics of molecules in extreme rotational states has been recently reported.[14]

Dissociation is an extreme example of coupled ro-vibrational dynamics. In view of coherent control of ro-vibrational dynamics, it is also interesting to understand the spread of population across the vibrational manifold below the dissociation limit. One of the open questions is whether the optical centrifuge can provide an experimental tool to make the molecule climb the vibrational ladder in a controlled way (much like it does with the rotational ladder climbing). Alternatively, one may ask whether high rotational excitation of molecules with low vibrational energies can be executed with the optical centrifuge in such a way as to keep their vibrational state intact, thus protecting them from potential dissociation. Heavier molecules may be susceptible to the vibrational excitation by the centrifuge field, leading to ro-vibrational coupling, which may significantly change the dynamics of a super-rotor.

Our aim here is to theoretically analyze the degree of vibrational excitation, comparing the effect of the centrifuge with that of a simple Gaussian pulse. To this end, we have

[a] *Departamento de Física Atómica, Molecular y Nuclear, Universidad de Granada, 18071 Granada, Spain. E-mail: rogonzal@ugr.es*
[b] *Department of Physics and Astronomy, The University of British Columbia, Vancouver, Canada*
[c] *Dahlem Center for Complex Quantum Systems and Fachbereich Physik, Freie Universität Berlin, Germany*
[d] *Instituto Carlos I de Física Teórica y Computacional, Universidad de Granada, 18071 Granada, Spain*

carried out a full quantum mechanical analysis of the rovibrational dynamics of a diatomic molecule in a non-resonant laser field. We compare a pulse whose time envelope mimics one of the polarization axes of an optical centrifuge[15] with a Gaussian pulse with the same spectral bandwidth and carrying the same energy as the centrifuge pulse. We have chosen Rb_2 as an example of a heavy diatomic molecule that can be prepared and studied in a trapped ultracold gas.[16–19]

This article is organized as follows. In Section 2, we describe the system Hamiltonian, including the interaction with the optical centrifuge and another non-resonant laser pulse. Section 3 is devoted to exploring the field-dressed dynamics of the rovibrational ground state and of several excited states as well as of a thermal sample. Conclusions and outlook are presented in Section 4.

2 System description and numerical method

We consider a diatomic molecule in the $a^3\Sigma^+$ electronic state exposed to a non-resonant laser pulse linearly polarized along the Z-axis of the laboratory-fixed frame (LFF). Within the Born–Oppenheimer approximation, the nuclear Hamiltonian is given by

$$H(t) = T_{\mathrm{R}} + \frac{\mathbf{N}^2}{2\mu R^2} + V(R) + H_I(t), \tag{1}$$

where the first and second terms stand for the vibrational and rotational kinetic energies, respectively, $\mathbf{N}$ is the rotational angular momentum, μ is the reduced mass of the molecule, R is the internuclear distance, and $V(R)$ is the electronic potential energy curve. For a non-resonant laser field, the polarizability interaction reads

$$H_I(t) = -\frac{I(t)}{2c\varepsilon_0}\left(\Delta\alpha(R)\cos^2\theta + \alpha_\perp(R)\right), \tag{2}$$

where $I(t)$ is the intensity of the laser field, c is the speed of light in a vacuum, ε_0 is the electric permitivity of vacuum, and θ is the Euler angle formed between the internuclear and laser polarization axes. The polarizability anisotropy is $\Delta\alpha(R) = \alpha_\parallel(R) - \alpha_\perp(R)$, with $\alpha_\parallel(R)$ and $\alpha_\perp(R)$ being the parallel and perpendicular components of the polarizability in the molecular-fixed frame (MFF).

The time-dependent Schrödinger equation associated with the Hamiltonian (1) is solved by a grid representation of the wave function, *i.e.*, the Fourier and discrete variable representations for the radial and angular coordinates, respectively,[20–22] and the time evolution is calculated using the Chebyshev propagator.[23] The field-dressed dynamics is analyzed in terms of the field-free rovibrational eigenstates of the Hamiltonian (1) (obtained by setting $t = 0$), $\Phi_{\nu,N,M_N}(\mathbf{R}) = \phi_{\nu,N}(R)Y_{N,M_N}(\theta, \varphi)$, where $\phi_{\nu,N}(R)$ and $Y_{N,M_N}(\theta, \varphi)$ are the vibrational and rotational parts, respectively, with $Y_{N,M_N}(\theta, \varphi)$ being the spherical harmonics, and (ν, N, M) the vibrational, rotational, and magnetic quantum numbers. For the sake of simplicity, we refer to the eigenstate $\Phi_{\nu,N,M_N}(\mathbf{R})$ by its quantum numbers (ν, N, M). For a given initial state $\Psi(\mathbf{R}, t = 0) = \Phi_{\nu_0,N_0,M_{N_0}}(\mathbf{R})$, the time-dependent wave function can be expressed as

$$\Psi(\mathbf{R}, t) = \sum_{\nu,N} C_{\nu_0,N_0,M_{N_0}}(\nu, N, t)\Phi_{\nu,N,M_N}(\mathbf{R}, t), \tag{3}$$

where the sum runs over all vibrational bands and rotational excitations up to a maximal value, which is chosen to ensure converged results. In this expansion (3), we have used that M_{N_0} is a good quantum number due to the azimuthal symmetry. The coefficients $C_{\nu_0,N_0,M_{N_0}}(\nu, N, t)$ depend on the time during the pulse duration. Afterwards, the Hamiltonian (1) becomes time-independent, and these coefficients acquire constant absolute values but varying phases.

We consider two different laser fields, both linearly polarized along the LFF Z-axis. The first one is a "two-dimensional" centrifuge pulse (CP), which mimics the experimental pulses used in ref. 24. While the two-dimensional model greatly simplifies our analysis, we expect its result to apply to conventional three-dimensional centrifuge fields,[15] because our focus is on the effects which do not depend on the directionality of molecular rotation. The intensity of this pulse is given by

$$I_{\mathrm{C}}(t) = \begin{cases} I_{\mathrm{C}}^0 \sin^2\left(\dfrac{\pi t}{2t_0}\right) g(t;\beta), & 0 \le t \le t_0, \\ I_{\mathrm{C}}^0 g(t;\beta), & t_0 < t \le t_{\mathrm{C}} - t_0, \\ I_{\mathrm{C}}^0 \sin^2\left(\dfrac{\pi(t_{\mathrm{f}} - t)}{t_0}\right) g(t;\beta), & t_{\mathrm{C}} - t_0 < t \le t_{\mathrm{C}}, \end{cases} \tag{4}$$

where I_{C}^0 is the peak intensity, t_0 the turning on and off time, and t_{C} the duration of this pulse. The function $g(t; \beta) = \sin^2(\beta t^2)$ simulates the oscillatory behavior of an experimental optical centrifuge pulse, with the parameter β being the analogue of the acceleration of the polarization axis rotation. Here, the CP parameters are fixed to $\beta = 0.3$ ps^{-2}, $t_0 = 3$ ps and $t_{\mathrm{C}} = 15$ ps.

The second pulse is a non-modulated Gaussian pulse (GP) with the same spectral bandwidth as the CP, and intensity

$$I_{\mathrm{G}}(t) = I_{\mathrm{G}}^0 \exp\left(-\frac{(t - t_{\mathrm{g}})^2}{\sigma^2}\right), \tag{5}$$

where I_{G}^0 is the peak intensity and $2\sigma\sqrt{\ln 2}$ is the full width at half maximum (FWHM). This GP possesses the same spectral bandwidth as the considered CP if σ is taken to be $\sigma = 0.142$ ps. In addition, we impose that both pulses carry the same energy, which happens when their peak intensities are related to one another as $I_{\mathrm{G}}^0 = 24.05 I_{\mathrm{C}}^0$. The GP is centered at $t_{\mathrm{g}} = 0.671$ ps, twice the value of the FWHM of the GP, so that the intensity at $t = 0$ ps is $\sim I_{\mathrm{G}}^0 \times 10^{-10}$ W cm^{-2}. The duration of this pulse is $t_{\mathrm{G}} = 2t_{\mathrm{g}}$ ps, *i.e.*, four times the GP FWHM. By fixing this value of t_{G}, we have ensured that the effects due to very small, but non-zero, laser fields at the beginning and end of the time-evolution are negligible.

3 Field-dressed rovibrational dynamics

We consider a Rb_2 molecule for which the lowest triplet electronic state $a^3\Sigma_u^+$ accommodates approximately 41 vibrational states with no rotational excitation, *i.e.*, $N = 0$. Note that due to the molecular symmetries, the $a^3\Sigma_u^+$ potential only accommodates rotational states of even parity. The number of bound rotational excitations decreases as the vibrational quantum number ν increases. For instance, the maximal values of the rotational quantum numbers are $N = 152$, 5 and 0 for the vibrational bands $\nu = 0$, 39 and 40, respectively. For the lowest vibrational band of Rb_2 in the $a^3\Sigma_u^+$ electronic state, the rotational constant is 0.0104 cm^{-1}, whereas the vibrational splitting is 12.8 cm^{-1}.

The interaction with the laser field, for moderate to strong intensities, is expected to lead to a significant hybridization of the rotational motion, followed by an impulsive alignment because their durations are significantly shorter than the Rb_2 rotational period of $\tau_B = 1.6$ ns. However, the field-induced dressed dynamics for the CP and GP should be different due to the very distinct time scales and ways in which the pulses transfer the same energy to the molecule.

3.1 Dynamics of the rovibrational ground state

We assume that Rb_2 is initially in its rovibrational ground state (0, 0, 0) and analyze the dressed dynamics by the time-evolution of the projections of the wavepacket into the field-free basis, *i.e.*, $|C_{0,0,0}(\nu, N, t)|^2$, presented in Fig. 1. We only plot the coefficients of the field-free states with $\nu = 0$, 1 and $N \leq 14$. For the G and C pulses, the peak intensities are fixed to $I_G^0 = 10^{12}$ W cm^{-2} and $I_C^0 = 4.158 \times 10^{10}$ W cm^{-2}, respectively. Due to the selection rules $\Delta N = \pm 2$ of the field interaction, (0, 2, 0) is the first state contributing to the field-dressed wavepacket, and immediately afterwards, higher rotational excitations are also populated. The weights $|C_{0,0,0}(0, N, t)|^2$ initially increase up to a maximum, keeping an oscillatory behavior till the end of the pulse when they reach a final constant value. For the CP, the oscillatory behavior of $|C_{0,0,0}(0, N, t)|^2$ is a bit more irregular due to the consecutive maxima of $I_C(t)$. The low values of the weights plotted in Fig. 1 indicate that many rotational excitations contribute to the wave function.

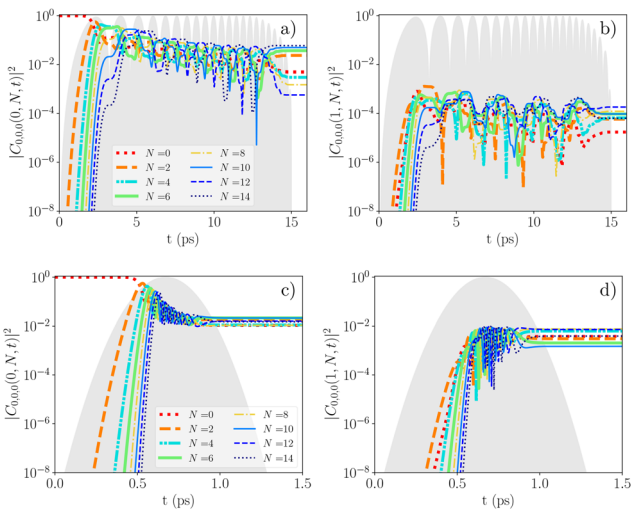

Fig. 1 For the initial state (0, 0, 0), time evolution of the weights of the field-free states $|C_{0,0,0}(\nu, N, t)|^2$ with rotational quantum number $N \leq 14$ and vibrational quantum numbers (a) and (c) $\nu = 0$; and (b) and (d) $\nu = 1$. The peak intensities are $I_G^0 = 10^{12}$ W cm^{-2} and $I_C^0 = 4.158 \times 10^{10}$ W cm^{-2}. The shaded areas represent the time profiles of the (a) and (b) centrifuge and (c) and (d) Gaussian pulses.

An interesting phenomenon is that both pulses provoke that states within neighboring vibrational bands get populated. The comparison between panels (b) and (d) of Fig. 1 shows that their contribution is more important for the GP-dressed wavepacket, but even so, they cannot be neglected for a proper description of the CP-induced dynamics. These non-zero weights of states with $\nu > 0$ prove a strong ro-vibrational coupling between the vibrational and rotational degrees of freedom, induced by the interaction with the non-resonant laser field, and the breakdown of the rigid-rotor approximation. The contribution of states from higher vibrational bands is also important at the end of the pulses, as shown by the weights of the field-free eigenstates plotted in Fig. 2(a) and (b) for the G and C pulses, respectively. These final weights illustrate the differences between the dynamics induced by these two fields. The distribution of population is wider in the vibrational and rotational quantum numbers for the GP-induced dynamics. For instance, the neighboring vibrational bands $\nu = 1$ and $\nu = 2$ have larger cumulative weights, defined in eqn (8), $\mathscr{V}_{0,0,0}(1, t = t_f) = 0.160$ and $\mathscr{V}_{0,0,0}(2, t = t_f) = 0.033$ due to the GP. In contrast, the vibrational distribution induced by the CP pulse is very narrow, with rather low cumulative weights, $\mathscr{V}_{0,0,0}(1, t = t_f) = 0.0018$ and $\mathscr{V}_{0,0,0}(2, t = t_f) = 0.0003$, which is due to its weaker peak intensity, and its gradual transfer of energy to the molecule. Indeed, the centrifuge time envelope enables a better control over the vibrational excitations that are not significantly increased after the first intensity maximum.

An experimental optical centrifuge creates molecular samples in super-rotor states, *i.e.*, in very high rotational excitations.[15] We analyze this property by the final cumulative weights in a certain rotational quantum number, independently of their vibrational band, $\mathscr{N}_{0,0,0}(N, t = t_f)$ defined in eqn (9). $\mathscr{N}_{0,0,0}(N, t = t_f)$ is plotted as a function of N in Fig. 3(a) and (b) for the G and C pulses, respectively. In addition, Fig. 3 shows the final weights in a certain

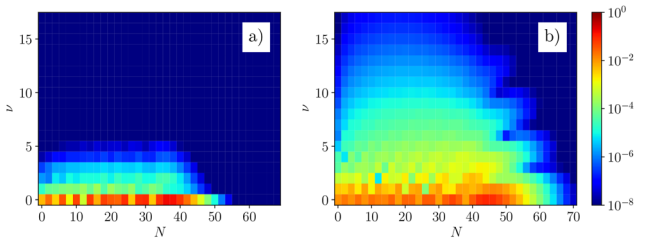

Fig. 2 For the initial state (0, 0, 0), final weights of the field-free rovibrational states $|C_{\nu,N}^0(t_f)|^2$ after the (a) centrifuge and (b) Gaussian pulses with peak intensities $I_C^0 = 4.158 \times 10^{10}$ W cm^{-2} and $I_G^0 = 10^{12}$ W cm^{-2}, respectively.

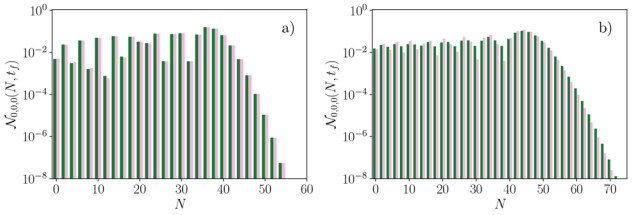

Fig. 3 For the initial state (0, 0, 0), final population distribution (dark green) according to rotational quantum number N defined in eqn (9) after the (a) centrifuge and (b) Gaussian pulses with peak intensities $I_C^0 = 4.158 \times 10^{10}$ W cm^{-2} and $I_G^0 = 10^{12}$ W cm^{-2}, respectively. For the rigid-rotor approximation (light pink), we present the weights of each rotational state with the lowest vibrational band $\nu = 0$.

rotational excitation obtained within the rigid-rotor description, see Appendix A. The GP-dressed dynamics involves many rotational excitations, $\mathscr{N}_{0,0,0}(N, t = t_f)$ shows small-amplitude oscillations as N increases and reaches a global maximum at $N = 44$, decreasing afterwards. The rigid-rotor approximation does not reproduce the rovibrational results due to the large contribution from neighboring vibrational bands. For the CP-induced dynamics, $\mathscr{N}_{0,0,0}(N, t = t_f)$ also oscillates with N having larger amplitudes, and reaches its global maximum at $N = 36$, approaching zero for higher values of N. For the CP case, rigid-rotor description provides a good approximation because the contributions from higher vibrational bands are rather small at the weak peak intensity of the CP. The mean rotational excitations, defined in eqn (10), are $\langle \mathscr{N}_{0,0,0} \rangle = 32.2$ and 27.6 for the GP and CP, respectively. These mean values indicate that the way energy is transferred by the GP pulse to the ground state gives rise to higher rotational excitations than in the CP dynamics.

Non-resonant light is normally used to produce samples of molecules aligned along the laser-polarization axis. The time evolution of the alignment $\langle \cos^2\theta \rangle \equiv \langle \Psi(R, t)|\cos^2\theta|\Psi(R, t)\rangle$ induced by these pulses is presented in Fig. 4. For comparison, the results obtained within the rigid-rotor approximation are also plotted in this figure. Both pulses provoke an impulsive alignment to the molecule due to their short duration compared to the molecular rotational period, with $\langle \cos^2\theta \rangle$ reaching extreme values at the rotational revivals $k\tau_B/4$, with k being an integer. For the GP-induced alignment, there are large deviations between the rigid-rotor and rovibrational descriptions, due to the important role played by higher vibrational bands on the dressed dynamics. For instance, the alignment obtained with the full rovibrational description possesses smaller maximal values, which are reduced and shifted with respect to the revivals $k\tau_B/4$ as time increases. For the CP-induced alignment, the agreement with the rigid-rotor description is good during (approximately) the first rotational period. Indeed, the narrow vibrational broadening induced by this pulse provokes that the differences between these results and a small reduction of the maximal alignment appear only at later times.

We conclude this section by analyzing the dynamics induced in the initial state (0, 0, 0) by a CP with a stronger intensity, $I_C^0 = 1.8 \times 10^{11}$ W cm^{-2}, the weights $|C_{0,0,0}(\nu, N, t)|^2$ are plotted in Fig. 5 at different times. Due to the stronger peak intensity, already at the first maximum, a significant population is transferred to the vibrational band $\nu = 1$. By further increasing the time, the distribution of population becomes significantly wider in N, but not in ν. At the end of the pulse, there are several vibrational bands with significant contributions, $\mathscr{V}_{0,0,0}(1, t = t_f) = 0.028$ and $\mathscr{V}_{0,0,0}(2, t = t_f) = 0.011$. However, despite these moderate vibrational weights, the CP pulse efficiently transfers population to higher rotational excitations, reaching the mean value $\left\langle \mathscr{N}_{\nu_0,N_0,M_{N_0}} \right\rangle = 32.8$.

3.2 Dynamics of rovibrational excited states

In this section, we analyze the impact of these two pulses on excited vibrational states, taking as a prototype example the initial state (25, 0, 0). Fig. 6 and 7 present the weights $|C_{25,0,0}(\nu, N, t)|^2$ as a function of ν and N at different time steps of the GP- and CP-dressed dynamics, respectively. The peak intensities are fixed to $I_G^0 = 10^{12}$ W cm^{-2} and $I_C^0 = 4.158 \times 10^{10}$ W cm^{-2}.

At the beginning of the pulses, the population distribution is similar, as illustrated in panels (a) of Fig. 6 and 7 for $t = 0.553$ ps

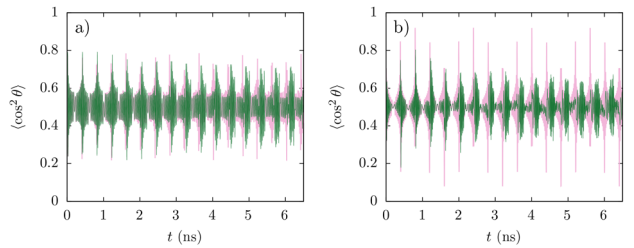

Fig. 4 For the initial state (0, 0, 0), time evolution of the alignment (dark-green thin line) induced by the (a) centrifuge and (b) Gaussian pulses with peak intensities $I_G^0 = 10^{12}$ W cm^{-2} and $I_C^0 = 4.158 \times 10^{10}$ W cm^{-2}, respectively. The alignment computed within the rigid-rotor (light-pink thick line) approximation is also plotted.

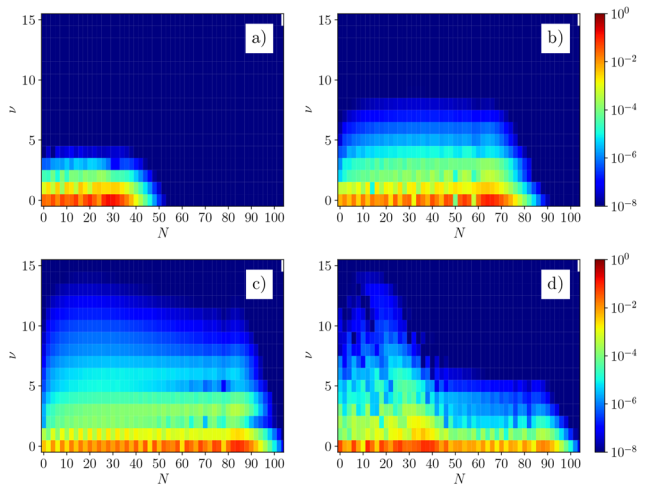

Fig. 5 For the initial state (0, 0, 0) in a CP, weights $|C_{0,0,0}(\nu, N, t)|^2$ of the field-free rotational and vibrational states into the field-dressed wavepacket at times (a) $t = 3.236$ ps (first maximum of $I_C(t)$); (b) $t = 5.605$ ps (third maximum); (c) $t = 7.926$ ps (sixth maximum); and (d) at the end of the pulse ($t = 15$ ps), with peak intensity $I_C^0 = 1.8 \times 10^{11}$ W cm^{-2}.

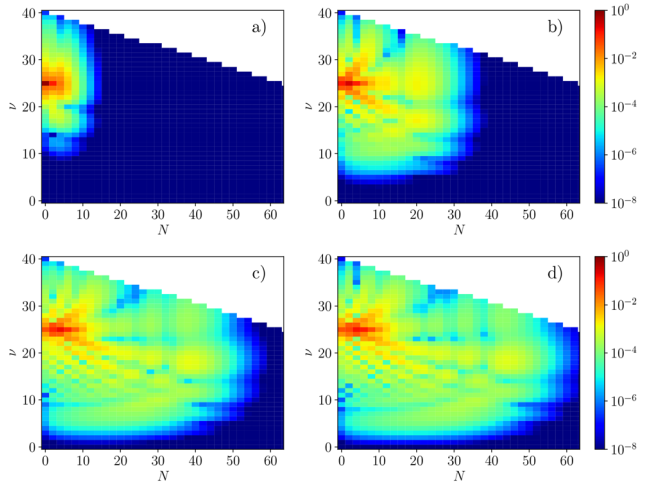

Fig. 6 For the initial state (25, 0, 0) in a GP, weights $|C_{25,0,0}(\nu, N, t)|^2$ of the field-free rotational and vibrational states into the field-dressed wavepacket (a) at the FWHM t = 553 fs; (b) at the maximum of the GP $t = t_g$ = 671 fs; (c) at the FWHM t = 790 fs; (d) and at the end of the GP. The peak intensity is $I_G^0 = 10^{12}$ W cm^{-2}.

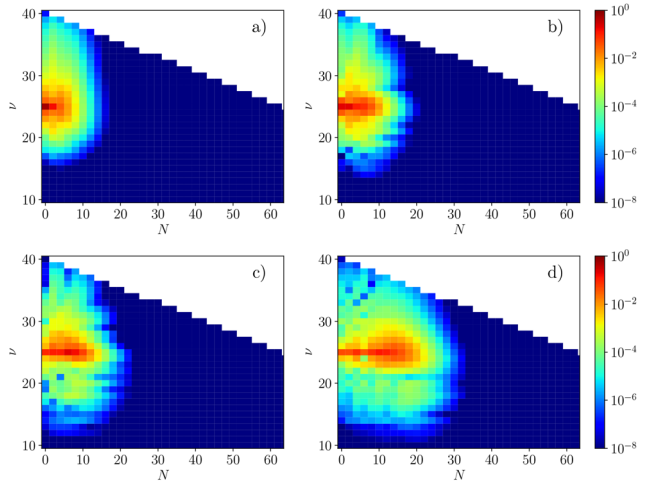

Fig. 7 For the initial state (25, 0, 0) in a CP, weights $|C_{25,0,0}(\nu, N, t)|^2$ of the field-free rotational and vibrational states in the field-dressed wavepacket at (a) first maximum t = 3.236 ps; (b) third maximum t = 5.605 ps; (c) sixth maximum t = 7.926 ps; and (d) at the end of the pulse t = 15 ps. Peak intensity is $I_C^0 = 4.158 \times 10^{10}$ W cm^{-2}.

and 3.236 ps, respectively. Initially, the rotational excitations within $\nu_0 = 25$ show the largest contribution to the wavepackets, but those within the neighboring vibrational bands $\nu_0 \pm 1$, 2 also possess significant weights. As time increases, the differences between the field-dressed dynamics become more evident and are due to the distinct ways that the pulses transfer energy to the molecule. The short duration and high intensity of the GP indicate that significantly more rovibrational states are involved in the dynamics, with a large amount of population transferred to other vibrational bands. This population distribution to neighboring vibrational bands follows a diagonal path due to that the dominant matrix elements between different bands: $\langle \nu, N, M_N|\Delta\alpha(R)\cos^2\theta|\nu \pm 1, N \pm 2, M_N\rangle$, see Fig. 12 for the radial part of this matrix element. For the CP wavepacket, more rotational excitations get populated at these later time steps, whereas the total weights of states in different vibrational bands does not change significantly after the first intensity maximum, being the main contributions from $\nu_0 \pm 1$, 2 and 3. This controlled spread over vibrational excitations reflects the gradual transfer of energy from the centrifuge field to the molecule. Hence, in this strong coupling regime, the CP pulse is more efficient in creating super-rotor wavepackets formed by high rotational excitations while simultaneously keeping a narrow distribution of vibrational bands.

Compared to the ground state, the impact on this excited state of these laser fields is weaker. This is due to the largest spatial extension of the vibrational wave function as ν increases, and the highest probability density being located close to the outermost classical turning point of the electronic potential curve. As a consequence, the overlaps of the corresponding wave functions with the R-dependent polarizabilities are smaller, reducing the impact of the laser field. In contrast to the ground-state, the CP is more efficient at climbing the rotational ladder, and at the end of the pulses, the mean values of the rotational excitations are $\langle \mathcal{N}_{25,0,0}\rangle$ = 10.35 and 7.90 for the C and G pulses, respectively. For the GP-dressed dynamics, the wider distribution of the final weights in the vibrational and rotational quantum numbers reduces the contributions of highly excited rotational states, and, as a consequence, the mean value $\langle \mathcal{N}_{25,0,0}\rangle$ becomes smaller.

Analogous results are obtained for other vibrational excited state (ν_0, 0, 0), as illustrated in Fig. 8 with the final distribution of population in the rovibrational spectrum for ν_0 = 5, 10, 35 and 39, and peak intensities $I_G^0 = 10^{12}$ W cm^{-2} and $I_C^0 = 4.158 \times 10^{10}$ W cm^{-2}. The dressed dynamics of these states shows similar features as those discussed for (25, 0, 0) above. For both pulses, we observe that as the vibrational excitation increases, the impact of the laser field is reduced. The stronger impact induced by the GP pulse, gives rise to higher hybridization of the rotational and vibrational motions, illustrated by wider distributions among the field-free states. Most important, the CP-induced vibrational spreading is very narrow for all analyzed cases.

We explore the creation of molecular samples in highly excited rotational states by the final mean value of the rotational excitation $\langle \mathcal{N}_{\nu_0,0,0}\rangle$ eqn (10), which is presented in Fig. 9 as a function of the vibrational excitation ν_0 and for several peak intensities of both pulses. As indicated above, the impact of the laser field decreases as ν_0 increases, which is manifested in the decreasing trend of $\langle \mathcal{N}_{\nu_0,0,0}\rangle$. For the lowest peak intensities, $\langle \mathcal{N}_{\nu_0,0,0}\rangle$ reaches similar values for both pulses. In contrast, for the strongest intensities, the rotational ladder is climbed more (less) efficiently by applying a CP than a GP for the rotational ground states in the vibrational bands with $\nu_0 \gtrsim 14$ ($\nu_0 \lesssim 14$). This is due to the broader vibrational distribution induced by the GP for these initial excited states, which reduces the weight of higher rotational excitations, and, therefore, the value of $\langle \mathcal{N}_{\nu_0,0,0}\rangle$. For the vibrational bands close to the

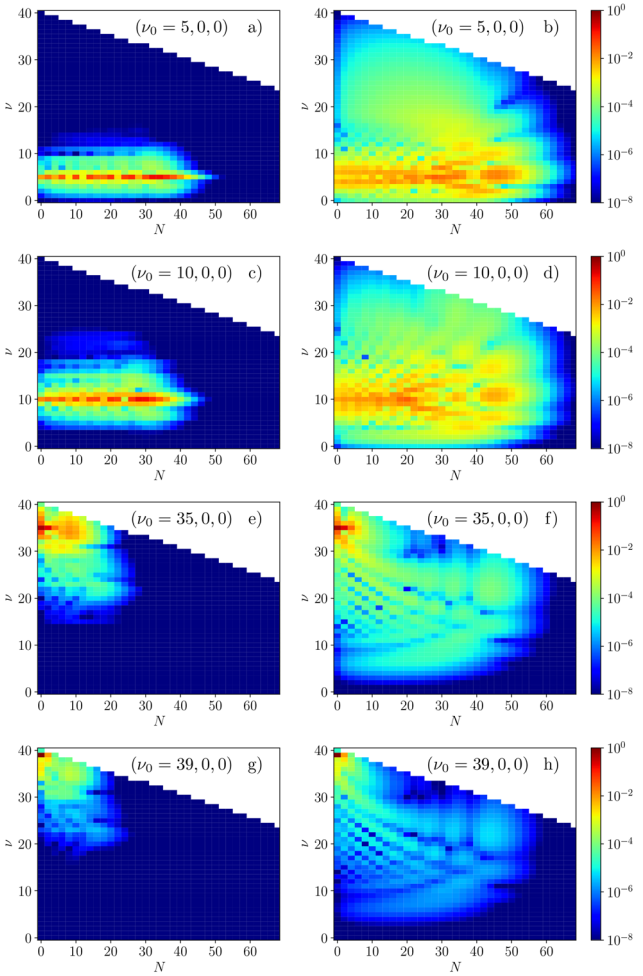

Fig. 8 For the initial states (ν_0, 0, 0), weights $|C_{\nu_0,0,0}(\nu, N, t)|^2$ of the field-free rotational and vibrational states in the field-dressed wavepacket at the end of the centrifuge (left column) and Gaussian (right column) pulses with peak intensity I_C^0 = 4.158 × 10^{10} W cm^{-2} and I_G^0 = 10^{12} W cm^{-2}, respectively.

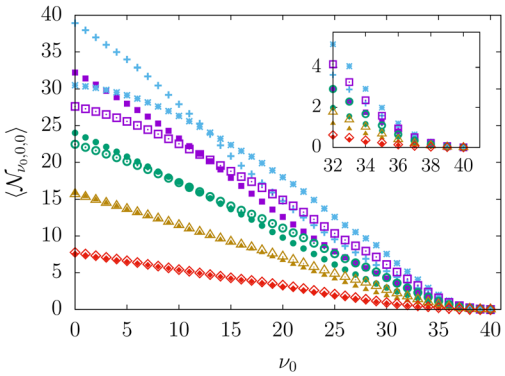

Fig. 9 The accumulative rotational weights at the end of a Gaussian and centrifuge pulse as a function of the vibrational quantum number of the initial states (ν_0, 0, 0). The inset shows these accumulative rotational weights for initial states close to the dissociation threshold with $\nu_0 \geq 32$. The peak intensities are fixed so that both pulses carry the same energy, and are I_C^0 = 50.00 GW cm^{-2} (blue stars), I_C^0 = 41.58 GW cm^{-2} (purple squares), I_C^0 = 31.18 GW cm^{-2} (green circles), I_C^0 = 20.79 GW cm^{-2} (yellow triangles) and I_C^0 = 10.39 GW cm^{-2} (red diamonds), for the centrifuge pulse; and I_G^0 = 1.203 TW cm^{-2} (blue crosses), I_G^0 = 1.00 TW cm^{-2} (purples filled squares), I_G^0 = 0.75 TW cm^{-2} (green filled circles), I_G^0 = 0.50 TW cm^{-2} (yellow filled triangles) and I_G^0 = 0.25 TW cm^{-2} (red filled diamonds) for the Gaussian pulse.

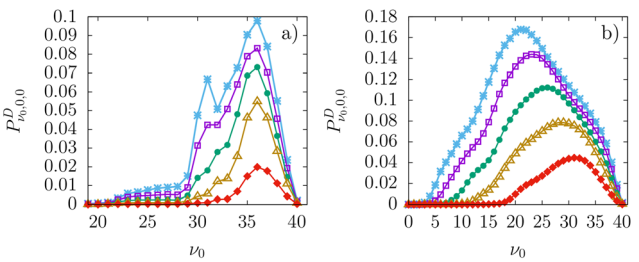

Fig. 10 For the initial states (ν_0, 0, 0), population transferred to the continuum eqn (11) at the end of the (a) centrifuge and (b) Gaussian pulses for several peak intensities: for the centrifuge, I_C^0 = 50.00 GW cm^{-2} (blue stars), I_C^0 = 41.58 GW cm^{-2} (purple squares), I_C^0 = 31.18 GW cm^{-2} (green filled circles), I_C^0 = 20.79 GW cm^{-2} (yellow triangles) and I_C^0 = 10.39 GW cm^{-2} (red filled diamonds), and for the Gaussian, I_G^0 = 1.203 TW cm^{-2} (blue stars), I_G^0 = 1.00 TW cm^{-2} (purple squares), I_G^0 = 0.75 TW cm^{-2} (green filled circles), I_G^0 = 0.50 TW cm^{-2} (yellow triangles) and I_G^0 = 0.25 TW cm^{-2} (red filled diamonds). These intensities have been taken so that both pulses carry the same energy, see Section 2.

dissociation threshold, $\langle \mathcal{N}_{\nu_0,0,0} \rangle$ reaches rather low values due to the small amount of rotational excitations bound in those bands and a weaker field impact.

An important feature of the dressed dynamics is the partial dissociation of the molecule, as scattering states also contribute to the final wave function.[25] This occurs for (25, 0, 0) in Fig. 7, and for ν_0 = 5, 10, 35 and 39 under the CP in Fig. 8. For all these states, we find that the uppermost rotational excitation bounded within a certain vibrational band is populated. This field-induced dissociation at the end of the pulse is quantified $P^D_{\nu_0,0,0}$, defined in eqn (11), which is plotted in Fig. 10(a) and (b) as a function of ν_0 and for several peak intensities of the G and C pulses, respectively. This field-induced dissociation strongly depends on the initial state, pulse shape and peak intensity. For the GP, $P^D_{\nu_0,0,0}$ shows a smooth behavior as a function of the vibrational band of the initial state ν_0. $P^D_{\nu_0,0,0}$ initially increases as ν_0 increases, reaching a maximum, and then decreases for highly excited vibrational bands. As the peak intensity increases, the largest amount of population is transferred to the continuum, and, in addition, the maximum is shifted to lower values of ν_0, being at ν_0 = 36 and ν_0 = 22 for I_G^0 = 2.5 × 10^{11} W cm^{-2} and 1.203 × 10^{12} W cm^{-2}, respectively. For the CP, the dependence of $P^D_{\nu_0,0,0}$ on ν_0 changes as I_C^0 increases, transforms from having only one maximum to two, being the global one located at ν_0 = 36 for all considered peak intensities I_C^0.

The narrower vibrational spreading induced by the CP pulse favors the reduction of the dissociation for most initial states. Indeed, the stronger vibrational impact of the GP is reflected in a higher value of $P^D_{\nu_0,0,0}$ for most of the analyzed states, except for the highly excited vibrational ones lying close to the

dissociation limit. For instance, for $\nu_0 = 36$, $P^{D}_{\nu_0,0,0} = 0.06$ and 0.08 for a GP with $I^0_G = 10^{12}$ W cm^{-2} and a CP with $I^0_C = 4.158 \times 10^{10}$ W cm^{-2}, respectively. For the GP, the ladder-like distribution of population implies that lower-lying vibrational bands are populated, and these bands accommodate more rotational excitations, thereforemaking the dissociation harder. In contrast, at the end of the CP, mainly neighboring vibrational bands to $\nu_0 = 36$ are populated, making it easier to reach their maximal rotational excitation and facilitating the molecular dissociation.

3.3 Thermal distribution

The results discussed in the previous sections assume either a rotational temperature of 0 K, *i.e.*, the (0, 0, 0) state, or vibrational excitations but no rotational excitation $N_0 = 0$. Molecular samples in a single rovibrational state are experimentally feasible in the ultracold regime.[26,27] However, molecular beam experiments are characterized by a certain rotational temperature, making it extremely challenging to create molecular samples in a single state.[28–30] Here, we consider thermal samples of Rb_2 with rotational temperatures that are experimentally feasible $T \leq 2.0$ K. In our description, the thermal sample is restricted to states within the lowest vibrational band, *i.e.*, with quantum numbers $(0, N, M_N)$ with $N \leq 24$ and $N \leq M_N \leq N$. Note that for $T = 2$ K, the weight of field-free states with rotational quantum number $N > 24$ is smaller than 0.01.

In Fig. 11, we present the thermal weights of the rotational excitations $\langle \mathcal{N} \rangle_T$, defined in eqn (12), at the end of the Gaussian and centrifuge pulses with peak intensities $I^0_G = 1.203 \times 10^{12}$ W cm^{-2} and $I^0_C = 5.0 \times 10^{10}$ W cm^{-2}, respectively. Note that at these intensities and for the initial states $(0, N, M_N)$, no population is transferred to the continuum. For both pulses, these thermal distributions are very similar. They show an increasing trend until reaching a maximum for $N = 54$ and 42 for the GP and CP, respectively. This demonstrates the creation of samples in highly excited rotational states such as super-rotors. As the temperature increases, these maxima are reduced due to the larger weights of higher rotational excitations to the thermal sample, for which the impact of the external fields is smaller.

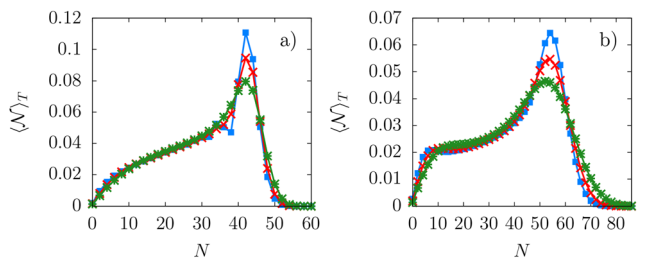

Fig. 11 For thermal samples of Rb_2 at rotational temperatures $T = 0.5$ K (blue squares), $T = 1.0$ K (red crosses) and $T = 2.0$ K (green stars), post-pulse distribution of the population among the rotational states eqn (10) for (a) a centrifuge pulse with $I^0_C = 5.0 \times 10^{10}$ W cm^{-2}, and (b) a Gaussian pulse with peak intensity $I^0_G = 1.203 \times 10^{12}$ W cm^{-2}.

4 Conclusions

We have explored the rovibrational dynamics of Rb_2 molecules in the $a^3\Sigma^+$ electronic state, due to non-resonant light. For the laser field, we have considered two different time envelopes having the same spectral bandwidth and carrying the same amount of energy, but inducing different dynamics. For experimentally feasible laser intensities, we find a strong coupling between the vibrational and rotational degrees of freedom. Despite the breakdown of the rigid-rotor approximation, these laser fields create wavepackets characterized by very high angular momenta. We find that the creation of these highly excited rotational excitations can result in the dissociation of the molecule even when initially in deeply bound states, in line with an earlier prediction.[10]

For both pulses, the lack of selection rules in the vibrational quantum number hinders the control over the vibrational bands being populated. As a consequence, the field-dressed dynamics involve states from lower and upper lying vibrational bands, with similar weights. However, a comparison of the dynamics for both pulses shows that the centrifuge one enables a better control over the vibrational excitations, creating a narrower distribution in this degree of freedom. Thus, the centrifuge field provokes the excitation of high rotational states while maintaining relatively low spread along the vibrational bands. This partial control over the vibrational excitations is due to the gradual transfer of energy from the centrifuge pulse to the molecule. Initially, when the centrifuge intensity is increased till the first maximum, a few neighboring vibrational bands get weakly populated, but this vibrational-rotational coupling is not significantly enhanced in the consecutive maxima. As a consequence, the centrifuge field is more efficient at creating super-rotor wavepackets with low impact on the vibrational motion. In contrast, the shorter duration of the Gaussian pulse implies that the energy is transferred faster to the molecule, and results in a stronger coupling between the vibrational and rotational motions. Thus, the amount of population that is accumulated in higher rotational excitations might be reduced, due to the larger role played by neighboring vibrational bands in the field-dressed dynamics.

The results of our work offer new perspectives on the utility of the optical centrifuge to control not only rotational, but also vibrational molecular dynamics. Our results provide guidance for, and we hope will advance, ultrafast spectroscopic studies in which the separation of the rotational and vibrational excitations by intense laser pulses is of importance.

Conflicts of interest

There are no conflicts of interest to declare.

Data availability

The data associated with this article have been uploaded to a repository which can be accessed through the following link: https://hdl.handle.net/10481/111162.

Appendices

A Rigid-rotor approximation

Within the rigid-rotor approximation, the Hamiltonian of a diatomic molecule in a non-resonant laser pulse linearly polarized along the LFF Z-axis, is given by

$$H^{\mathrm{R}}(t) = \frac{\mathbf{N}^2}{2\mu}\langle R^{-2}\rangle_{\nu} + H_I^{\mathrm{R}}(t) \tag{6}$$

where the first term stands for the rotational kinetic energies, with the rotational constant given by $B_\nu = \frac{\hbar^2\langle R^{-2}\rangle_\nu}{2\mu}$. The interaction of the non-resonant light with the polarizability reads

$$H_I^{\mathrm{R}}(t) = -\frac{I(t)}{2c\varepsilon_0}\left(\langle\Delta\alpha(R)\rangle_\nu \cos^2\theta + \langle\alpha_\perp(R)\rangle_\nu\right). \tag{7}$$

The matrix elements $\langle f(R)\rangle_\nu = \langle\phi_{\nu,0}|f(R)|\phi_{\nu,0}\rangle_\nu$, with $f(R) = R^{-2}$, $\Delta\alpha(R)$ and $\alpha_\perp(R)$, and $\phi_{\nu,0} = \phi_{\nu,0}(R)$, the field-free vibrational wave function, adapt this approximation to the different vibrational bands of the molecular spectrum.[31] The time-dependent Schrödinger equation associated with Hamiltonian eqn (6) is solved by the short iterative Lanczos algorithm for the time propagation[21] and a basis set expansion in terms of the spherical Harmonics for the angular coordinates.[32]

B Weights and matrix elements

The field-dressed dynamics is analyzed by projecting the wave packet onto the basis formed by the field-free eigenstates of the electronic state $a^3\Sigma^+$ of Rb_2 as in eqn (3). For a given initial state (ν_0, N_0, M_{N_0}), the weight of the eigenstate (ν, N, M_{N_0}) to the field-dressed wave function is $\left|C_{\nu_0,N_0,M_{N_0}}(\nu,N,t)\right|^2$. To illustrate the breakdown of the rigid-rotor approximation, we calculate the population transferred to a certain vibrational band ν as

$$\mathscr{V}_{\nu_0,N_0,M_{N_0}}(\nu,t) = \sum_{N=0}^{N_{\max}}\left|C_{\nu_0,N_0,M_{N_0}}(\nu,N,t)\right|^2 \tag{8}$$

where $N_{\max}$ is the maximum number of rotational states included in the basis set expansion (3). Analogously, an accumulative rotational distribution, independent of the vibrational excitations, can be defined as

$$\mathscr{N}_{\nu_0,N_0,M_{N_0}}(N,t) = \sum_{\nu}\left|C_{\nu_0,N_0,M_{N_0}}(\nu,N,t)\right|^2 \tag{9}$$

where the sum runs over all vibrational bands of the Rb_2 $a^3\Sigma^+$ electronic state. At the pulses, we compute the mean value of the rotational excitations defined as

$$\left\langle\mathscr{N}_{\nu_0,N_0,M_{N_0}}\right\rangle = \frac{\sum_{N=0}^{N_{\max}} N\mathscr{N}_{\nu_0,N_0,M_{N_0}}(N,t_{\mathrm{f}})}{\sum_{N=0}^{N_{\max}}\mathscr{N}_{\nu_0,N_0,M_{N_0}}(N,t_{\mathrm{f}})}. \tag{10}$$

with $t_{\mathrm{f}} = t_{\mathrm{G}}$ and t_{C} for the GP and CP, respectively. These expressions (8)–(10) take into account that M_{N_0} is a good quantum number due to the azimuthal symmetry.

Due to the strong field impact, part of the population is transferred to scattering states, *i.e.*, to the continuum. This effect is quantified by

$$P^{D}_{\nu_0,N_0,M_{N_0}} = 1 - \sum_{\nu,N}\left|C_{\nu_0,N_0,M_{N_0}}(\nu,N,t_{\mathrm{f}})\right|^2 \tag{11}$$

at the end of the G and C pulses, *i.e.*, $t_{\mathrm{f}} = t_{\mathrm{G}}$ and t_{C}, respectively. The sum in eqn (11) runs over all vibrational bands, and all rotational excitations included in the numerical treatment.

For a molecular sample at temperature T, the thermal average of the rotational excitations reads as

$$\langle\mathscr{N}\rangle_T = \sum_{\nu_0,N_0M_{N_0}}\mathscr{N}_{\nu_0,N_0,M_{N_0}}(N,t_{\mathrm{f}})W_{\nu_0N_0|M_{N_0}|}, \tag{12}$$

with $t_{\mathrm{f}} = t_{\mathrm{G}}$ and t_{C} for the GP and CP, respectively. The Maxwell–Boltzmann weights are

$$W_{\nu_0N_0|M_{N_0}|} = \frac{g_{|M_{N_0}|}\mathrm{e}^{\frac{E_{0,0}-E_{\nu_0,N_0}}{Tk_{\mathrm{B}}}}}{Z}, \tag{13}$$

where k_{B} is the Boltzmann constant, and $E_{0,0}$ and E_{ν_0,N_0} are the field-free energies of the (0, 0, 0) and (ν_0, N_0, M_{N_0}) states, respectively. The factor $g_{M_{N_0}}$ takes into account that the impact of the laser field on the states $(\nu_0, N_0, |M_{N_0}|)$ and $(\nu_0, N_0, -|M_{N_0}|)$ is identical, so that $g_0 = 1$ and $g_{|M_{N_0}|} = 2$ for $|M_{N_0}| \neq 0$. The normalization constant is given by

$$Z = \sum_{N_0=0}^{N_T}(2N_0+1)\mathrm{e}^{\frac{E_{0,0}-E_{\nu_0,N_0}}{Tk_{\mathrm{B}}}}, \tag{14}$$

where $(2N_0 + 1)$ is the field-free degeneracy in the magnetic quantum number. The highest rotational excitation included is $N_T \leq 24$. For the considered temperatures, we neglect the contribution of states in excited vibrational bands, restricting $\nu_0 = 0$ in eqn (13) and (14). Indeed, the thermal weight for the state (1, 0, 0), *i.e.*, the rotational ground state of the first excited vibrational band, is $W_{1,0,0} = 5.9 \times 10^{-18}$ and 1.5×10^{-6}, for $T = 0.5$ K and $T = 2$ K, respectively.

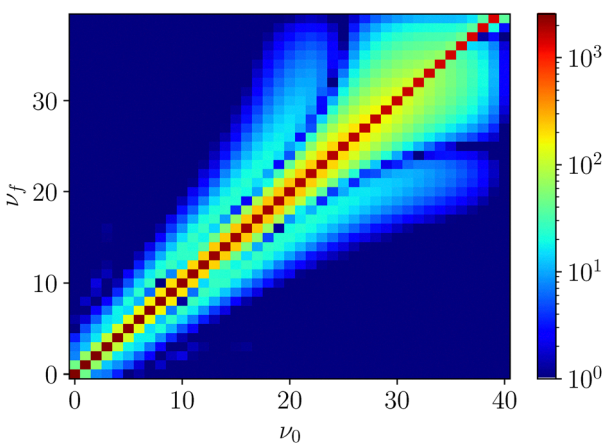

Fig. 12 Matrix elements of the vibrational part of the interaction eqn (15) between the states $(\nu_0, 0, 0)$ and $(\nu_f, 2, 0)$.

To better understand the mechanism behind the population transferred to other vibrational bands, Fig. 12 shows the radial matrix elements

$$|\langle \nu, 0|\Delta\alpha(R)|\nu', 2\rangle| = \left|\int \phi^*_{\nu,0}(R)\Delta\alpha(R)\phi_{\nu',2}(R)R^2 \mathrm{d}R\right|, \quad (15)$$

for the non-diagonal terms in the angular operator $\cos^2\theta$, *i.e.*, $\Delta N = \pm 2$.

Acknowledgements

Financial support from the Spanish projects PID2023-147039NB-I00 (MICIN), the Andalusian research group FQM-207 and the Deutsche Forschungsgemeinschaft through the joint ANR-DFG CoRoMo Projects no. 505622963 (KO 2301/15-1) is acknowledged. J. M. G. G. also acknowledges financial support from the grant PRE2021-099603 funded by MICIU/AEI/10.13039/501100011033 and by "ESF+".

Notes and references

1 H. Stapelfeldt and T. Seideman, *Rev. Mod. Phys.*, 2003, **75**, 543–557.
2 Y. Ohshima and H. Hasegawa, *Int. Rev. Phys. Chem.*, 2010, **29**, 619–663.
3 S. Fleischer, Y. Khodorkovsky, E. Gershnabel, Y. Prior and I. S. Averbukh, *Isr. J. Chem.*, 2012, **52**, 414–437.
4 C. P. Koch, M. Lemeshko and D. Sugny, *Rev. Mod. Phys.*, 2019, **91**, 035005.
5 J. Karczmarek, J. Wright, P. Corkum and M. Ivanov, *Phys. Rev. Lett.*, 1999, **82**, 3420–3423.
6 D. M. Villeneuve, S. A. Aseyev, P. Dietrich, M. Spanner, M. Y. Ivanov and P. B. Corkum, *Phys. Rev. Lett.*, 2000, **85**, 542–545.
7 I. MacPhail-Bartley, W. W. Wasserman, A. A. Milner and V. Milner, *Rev. Sci. Instrum.*, 2020, **91**, 045122.
8 A. S. Mullin, *Annu. Rev. Phys. Chem.*, 2025, **76**, 357–377.
9 J. Li, J. T. Bahns and W. C. Stwalley, *J. Chem. Phys.*, 2000, **112**, 6255–6261.
10 M. Spanner and M. Y. Ivanov, *J. Chem. Phys.*, 2001, **114**, 3456–3464.
11 C. Chandre and J. P. Salas, *Phys. Rev. A*, 2023, **107**, 063105.
12 M. Lemeshko and B. Friedrich, *Phys. Rev. Lett.*, 2009, **103**, 053003.
13 R. González-Férez and C. P. Koch, *Phys. Rev. A: At., Mol., Opt. Phys.*, 2012, **86**, 063420.
14 T. Y. Chen, S. A. Steinmetz, B. D. Patterson, A. W. Jasper and C. J. Kliewer, *Nat. Commun.*, 2023, **14**, 3227.
15 A. Korobenko, A. A. Milner and V. Milner, *Phys. Rev. Lett.*, 2014, **112**, 113004.
16 F. Lang, K. Winkler, C. Strauss, R. Grimm and J. H. Denschlag, *Phys. Rev. Lett.*, 2008, **101**, 133005.
17 M. Deiß, B. Drews, B. Deissler and J. Hecker Denschlag, *Phys. Rev. Lett.*, 2014, **113**, 233004.
18 J. Wolf, M. Deiß and J. Hecker Denschlag, *Phys. Rev. Lett.*, 2019, **123**, 253401.
19 X. He, K. Wang, J. Zhuang, P. Xu, X. Gao, R. Guo, C. Sheng, M. Liu, J. Wang, J. Li, G. V. Shlyapnikov and M. Zhan, *Science*, 2020, **370**, 331–335.
20 R. Kosloff, *J. Phys. Chem.*, 1988, **92**, 2087–2100.
21 M. Beck, A. Jackle, G. Worth and H.-D. Meyer, *Phys. Rep.*, 2000, **324**, 1–105.
22 J. C. Light and T. Carrington, *Adv. Chem. Phys.*, 2007, **114**, 263–310.
23 R. Kosloff, *Annu. Rev. Phys. Chem.*, 1994, **45**, 145–178.
24 A. A. Milner, A. Korobenko and V. Milner, *Phys. Rev. A*, 2016, **93**, 053408.
25 M. Lemeshko and B. Friedrich, *Phys. Rev. Lett.*, 2009, **103**, 053003.
26 S. Ospelkaus, K.-K. Ni, G. Quéméner, B. Neyenhuis, D. Wang, M. H. G. de Miranda, J. L. Bohn, J. Ye and D. S. Jin, *Phys. Rev. Lett.*, 2010, **104**, 030402.
27 P. K. Molony, P. D. Gregory, Z. Ji, B. Lu, M. P. Köppinger, C. R. Le Sueur, C. L. Blackley, J. M. Hutson and S. L. Cornish, *Phys. Rev. Lett.*, 2014, **113**, 255301.
28 L. Holmegaard, J. H. Nielsen, I. Nevo, H. Stapelfeldt, F. Filsinger, J. Küpper and G. Meijer, *Phys. Rev. Lett.*, 2009, **102**, 023001.
29 I. Nevo, L. Holmegaard, J. H. Nielsen, J. L. Hansen, H. Stapelfeldt, F. Filsinger, G. Meijer and J. Küpper, *Phys. Chem. Chem. Phys.*, 2009, **11**, 9912–9918.
30 J. S. Kienitz, S. Trippel, T. Mullins, K. Dlugolecki, R. González-Férez and J. Küpper, *ChemPhysChem*, 2016, **17**, 3740–3746.
31 R. González-Férez and P. Schmelcher, *Phys. Rev. A: At., Mol., Opt. Phys.*, 2004, **69**, 023402.
32 J. J. Omiste and R. González-Férez, *Phys. Rev. A: At., Mol., Opt. Phys.*, 2013, **88**, 033416.

